JACS
JOURNAL OF THE AMERICAN CHEMICAL SOCIETY
Article
pubs.acs.org/JACS

Fine-Tuning of Crystal Packing and Charge Transport Properties of BDOPV Derivatives through Fluorine Substitution

Jin-Hu Dou,[†,§] Yu-Qing Zheng,[†,§] Ze-Fan Yao,[†] Zhi-Ao Yu,[†] Ting Lei,[†] Xingxing Shen,[‡] Xu-Yi Luo,[†] Junliang Sun,[†] Shi-Ding Zhang,[†] Yi-Fan Ding,[†] Guangchao Han,[‡] Yuanping Yi,*[,‡] Jie-Yu Wang,*[,†] and Jian Pei*[,†]

[†]Beijing National Laboratory for Molecular Sciences (BNLMS), Key Laboratory of Bioorganic Chemistry and Molecular Engineering of the Ministry of Education, Center of Soft Matter Science and Engineering, College of Chemistry and Molecular Engineering, Peking University, Beijing 100871, China

[‡]Key Laboratory of Organic Solids, Institute of Chemistry, Chinese Academy of Sciences, Beijing 100190, China

Supporting Information

ABSTRACT: Molecular packing in organic single crystals greatly influences their charge transport properties but can hardly be predicted and designed because of the complex intermolecular interactions. In this work, we have realized systematic fine-tuning of the single-crystal molecular packing of five benzodifurandione-based oligo(*p*-phenylenevinylene) (BDOPV)-based small molecules through incorporation of electronegative fluorine atoms on the BDOPV backbone. While these molecules all exhibit similar column stacking configurations in their single crystals, the intermolecular displacements and distances can be substantially modified by tuning of the amounts and/or the positions of the substituent fluorine atoms. Density functional theory calculations showed that the subtle differences in charge distribution or electrostatic potential induced by different fluorine substitutions play an important role in regulating the molecular packing of the BDOPV compounds. Consequently, the electronic couplings for electron transfer can vary from 71 meV in a slipped stack to 201 meV in a nearly cofacial antiparallel stack, leading to an increase in the electron mobility of the BDOPV derivatives from 2.6 to 12.6 $cm^2 V^{-1} s^{-1}$. The electron mobility of the five molecules did not show a good correlation with the LUMO levels, indicating that the distinct difference in charge transport properties is a result of the molecular packing. Our work not only provides a series of high-electron-mobility organic semiconductors but also demonstrates that fluorination is an effective approach for fine-tuning of single-crystal packing modes beyond simply lowering the molecular energy levels.

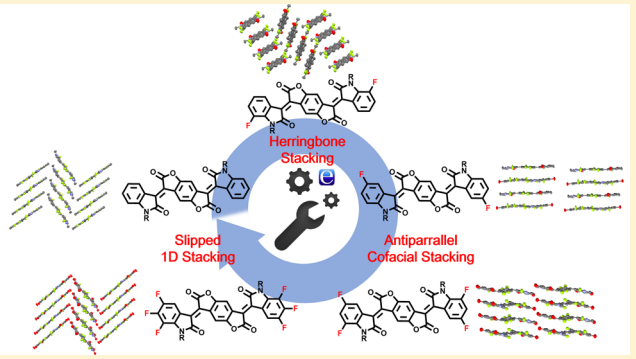

INTRODUCTION

Molecular packing in organic materials greatly influences the electronic coupling and therefore the charge transport process in organic light-emitting diodes (OLEDs), organic photovoltaics (OPVs), and organic field-effect transistors (OFETs).[1−8] Charge transport at the molecular level is mainly determined by two factors: the electronic coupling and the reorganization energy.[9] The electronic coupling (absolute value of the transfer integral) is strongly dependent on the molecular packing mode.[10,11] To obtain a large transfer integral, short $\pi-\pi$ stacking distances and optimal displacements are desired.[9−11] Several design strategies have been developed to alter the packing of organic molecules, such as extension of π conjugation to enhance the $\pi-\pi$ interactions between adjacent molecules,[12−14] incorporation of heteroatoms into the conjugated backbone to provide more non-covalent interactions (e.g., S−S and N−H$\cdots\pi$ interactions),[15−18] and substitution with bulky groups.[19−22] For example, incorporating appropriate bulky solubilizing groups at the peri position of pentacene can cause the molecular packing to adjust from a herringbone arrangement to a slipped brick wall arrangement[23] as a result of both a large increase in the stabilized dispersion interaction[24] and the steric hindrance effect of the bulky substituents. However, most reported organic small molecules with high carrier mobility, including pentacene,[12] [1]benzothieno[3,2-*b*]benzothiophene (BTBT),[25] and dianthra[2,3-*b*:2′,3′-*f*]-thieno[3,2-*b*]thiophene (DATT),[13] α-phase *N*,*N*′-bis-(heptafluorobutyl)-2,6-dichloro-1,4,5,8-naphthalenetetracarboxylic diimide (α-phase Cl_2-NDI),[26] etc., adopt herringbone arrangements instead of one-dimensional (1D) or brick-layer stacking (Figure S1). The fact that molecules with 1D or brick-layer stacking did not show the expected good device performance is mainly due to the large displacements induced

Received: October 28, 2015
Published: November 30, 2015

DOI: 10.1021/jacs.5b11114
J. Am. Chem. Soc. 2015, 137, 15947−15956

by the steric effect of bulky groups substituted on the axis of symmetry, such as triisopropylsilyl (TIPS)-pentacene and β-phase Cl_2-NDI (Figure 1b).[1,11,26−28] We envisioned that if bulky groups are introduced in a staggered fashion on the backbone to avoid the steric effect, molecules may adopt either slipped stacking or antiparallel cofacial stacking (Figure 1d,e). Since small chemical modifications can often lead to significant changes in crystal packing motifs,[29−31] it is extremely difficult to obtain an ideal system with subtle changes of molecular structure and crystal packing for structure−property relationship investigations. Therefore, in order to further improve the mobilities for the existing high-performance core structures and comprehensively understand the influence of solid-state packing, it is of great importance to find an appropriate modification method to fine-tune the molecular crystal packing.

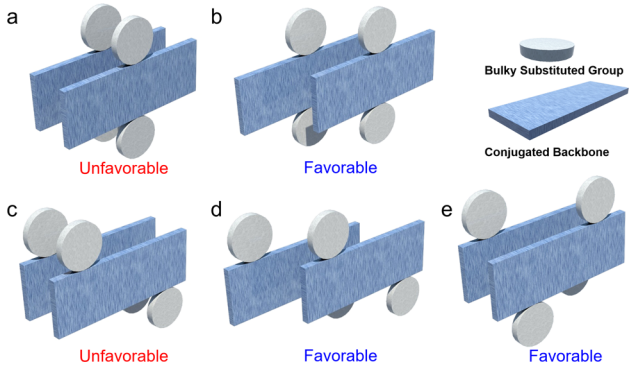

Figure 1. Diagram of molecular packing motifs. For bulky groups substituted on the axis of symmetry, (a) cofacial packing is unfavorable and (b) slipped stacking is favorable (example: TIPS-pentacene). For bulky groups substituted on the backbone in a staggered fashion, (c) cofacial stacking is unfavorable while (d) slipped stacking and (e) antiparallel stacking are favorable.

Fluorine atoms are frequently introduced into organic molecules to effectively lower their frontier orbital levels as a result of the strong electron-withdrawing properties of fluorine.[29,32−34] For example, fluorination of tetraceno[2,3-*b*]thiophene allowed systematic tuning of the energy levels in a series of molecules and realized the transition of charge carrier type from hole-only to ambipolar or electron-only transport because of the reduced electron injection barrier.[35] On the other hand, as fluorine atom has the largest Pauling electronegativity,[36,37] fluorination of organic semiconductors, especially on conjugated polymers, is beneficial for the formation of intramolecular hydrogen bonds to realize a rigid, planar backbone and thus high intrachain transport.[38] However, there is a lack of systematic and detailed studies of the effects of fluorination beyond the energy level modulation and conformation locking.[39−41]

Recently, materials based on benzodifurandione-based oligo(*p*-phenylenevinylene) (BDOPV), an electron-deficient conjugated backbone, presented high electron mobility and good environmental stability.[42−44] Utilizing this type of structure, we developed a new n-type small molecule, 2-ethylhexane (EH)-substituted BDOPV (Figure 2), which showed a slipped 1D stacking single-crystal structure and an electron mobility as high as 3.25 $cm^2\ V^{-1}\ s^{-1}$. To further lower the lowest unoccupied molecular orbital (LUMO) level as well as fine-tune the molecular packing mode, different amounts of electronegative fluorine atoms at different positions were incorporated into BDOPV to obtain four other n-type small molecules, *o*-F_2-BDOPV, *p*-F_2-BDOPV, F_4-BDOPV, and F_6-BDOPV (Figure 2). The single crystals of the five compounds all show similar column stacking with face-to-face interactions because they have the same conjugated backbone structures with large π planes. However, distinct intermolecular displacements and distances are found, which are largely attributed to subtle modulation of the molecular electrostatic potentials by fluorine substitution. In particular, benefiting from both the opposite electrostatic potentials on the lateral periphery and the

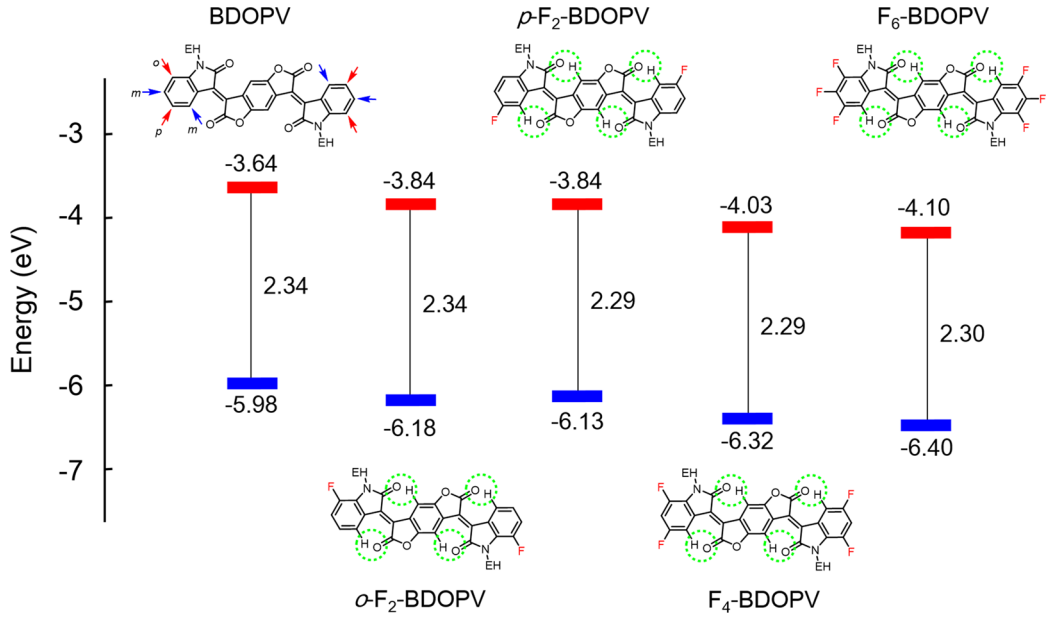

Figure 2. Chemical structures and B3LYP/6-311G(d,p)-calculated HOMO/LUMO levels of the five BDOPV derivatives. The arrows on BDOPV indicate the possible substitution positions of fluorine atoms. The circles on the molecules indicate the intermolecular hydrogen bonding between carbonyl and hydrogen atoms.

DOI: 10.1021/jacs.5b11114
J. Am. Chem. Soc. 2015, 137, 15947−15956

Scheme 1. Synthetic Approach to the Five BDOPV Derivatives

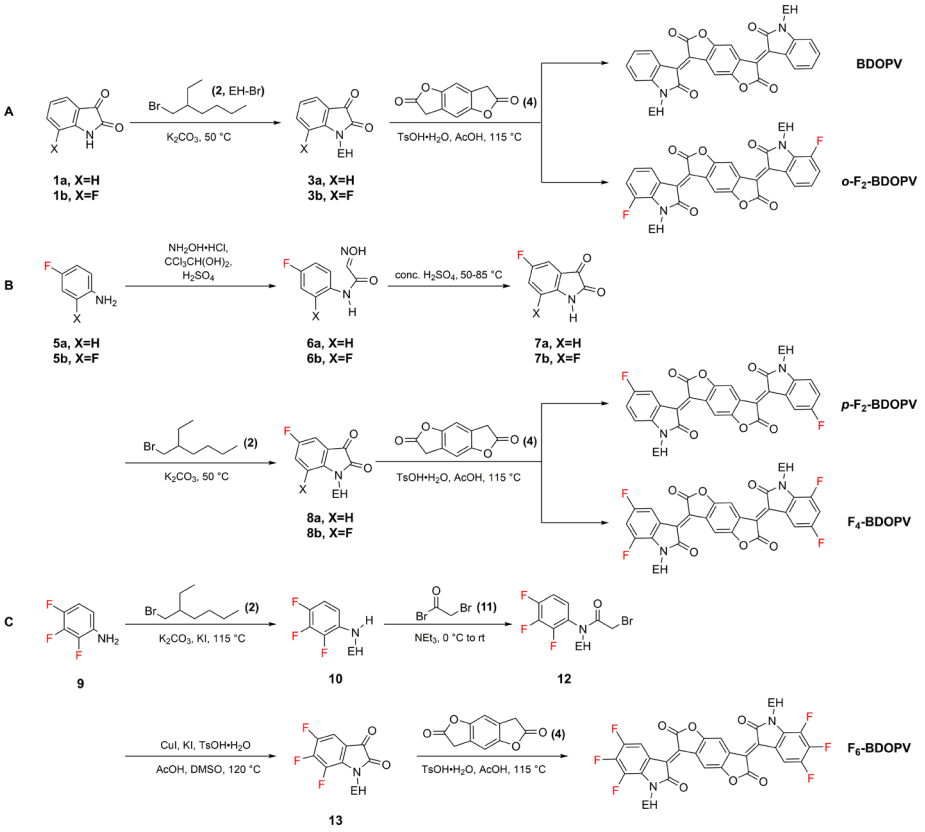

staggered positions of the substituted alkyl chains, *p*-F_2-BDOPV and F_4-BDOPV crystallize in an antiparallel cofacial stacking mode with tiny displacements, resulting in higher electron mobilities.

RESULTS AND DISCUSSION

Synthesis and Physical Properties. Scheme 1 illustrates the synthetic route to the five BDOPV derivatives.[44,45] For BDOPV and *o*-F_2-BDOPV, alkyl bromide **2** was used to introduce EH onto the commercially available compounds **1a** and **1b** as the side chain to offer good solubility. Compounds **3a** and **3b** were reacted with benzo[1,2-*b*:4,5-*b*′]difuran-2,6(3*H*,7*H*)-dione (**4**) to provide the target molecules BDOPV and *o*-F_2-BDOPV. For *p*-F_2-BDOPV and F_4-BDOPV, compounds **5a** and **5b** were condensed with chloral hydrate and hydroxylamine hydrochloride under acidic conditions, producing compounds **6a** and **6b**, which underwent a cyclization reaction using concentrated H_2SO_4 to afford compounds **7a** and **7b**. Then the EH side chains were introduced using **2** to offer good solubility. Compounds **8a** and **8b** were reacted with compound **4**, providing the target molecules *p*-F_2-BDOPV and F_4-BDOPV, respectively. For F_6-BDOPV, we first alkylated 2,3,4-trifluoroaniline (**9**) to obtain *N*-(2-ethylhexyl)-2,3,4-trifluoroaniline (**10**) and then treated the product with 2-bromoacetyl bromide (**11**) and NEt_3 to procure 2-bromo-*N*-(2-ethylhexyl)-*N*-(2,3,4-trifluorophenyl)-acetamide (**12**). Finally, we improved and refined a previously reported procedure to use CuI, KI, TsOH·H_2O, and AcOH as catalysts and dimethyl sulfoxide (DMSO) as the solvent and oxidant at 120 °C with a pump pumping air into the reaction system continually for 48 h to obtain the target molecule F_3-isatin-EH (**13**).[46] Then we followed the aldol reaction to get F_6-BDOPV from compounds **4** and **13**. Detailed synthetic procedures and data are shown in the Supporting Information.

All of the target molecules showed excellent thermal stability, with decomposition temperatures over 330 °C (Figure S3). Cyclic voltammetry (CV) was performed to evaluate the electrochemical properties of all five BDOPV derivatives both in solution and in thin films (Figure S6). The fluorinated BDOPV molecules show significantly lower highest occupied molecular orbital (HOMO) and LUMO energy levels compared with BDOPV both in solution and in the solid state, which is in accordance with the results of theoretical calculations (Figures 2 and S2). The band gaps calculated from the CV profiles of the solid-state compounds become smaller as the number of fluorine atoms increases. The LUMO levels of F_4-BDOPV and F_6-BDOPV in the solid state as obtained by CV are −4.44 eV, which is 0.48 eV lower than that of BDOPV. Furthermore, the five BDOPV molecules also show excellent reductive stability with two reversible redox couples in solution (Figure S6), suggesting their potential applications as electron-accepting and -transporting materials. The absorption spectra of the five BDOPV derivatives in dilute solution and in thin films are displayed in Figure S5. The band gaps calculated from the onsets of the absorption profiles in solution were around 1.8 eV for the five BDOPV derivatives, which is in accordance with the values obtained from the CV profiles. All of the molecules show high melting points in the range of 200−256 °C (Figure S4), indicating their good thermal stability. All of the photophysical and electrochemical data are summarized in Table S1.

Single-Crystal Packing and Analysis. Single crystals of all five BDOPV molecules were obtained by the slow solvent vapor diffusion method.[47] As can be seen from the scanning

DOI: 10.1021/jacs.5b11114
J. Am. Chem. Soc. 2015, 137, 15947−15956

Table 1. Crystallographic Packing Data for the Five Molecules

	BDOPV	*o*-F_2-BDOPV	*p*-F_2-BDOPV	F_4-BDOPV	F_6-BDOPV
crystal system	trigonal	triclinic	triclinic	triclinic	trigonal
space group	$R\bar{3}$	$P\bar{1}$	$P\bar{1}$	$P\bar{1}$	$R\bar{3}$
calculated density (g cm^{-3})	1.289	1.364	1.358	1.377	1.418
pitch angle (deg)[a]	54.9	46.9	22.5	9.9	57.8
roll angle (deg)[a]	20	31.1	17.6	10.1	13.5
longitudinal shift d_p (Å)[a]	4.88	3.47	1.41	0.587	5.38
transverse shift d_r (Å)[a]	1.25	1.98	1.08	0.601	0.81
slipping angle (deg)[a]	35.1	43.1	67.5	80.1	32.2
interplanar distance (Å)	3.43	3.25	3.41/3.43	3.36/3.38	3.39

[a]Calculated according to the method shown in Figure S11.

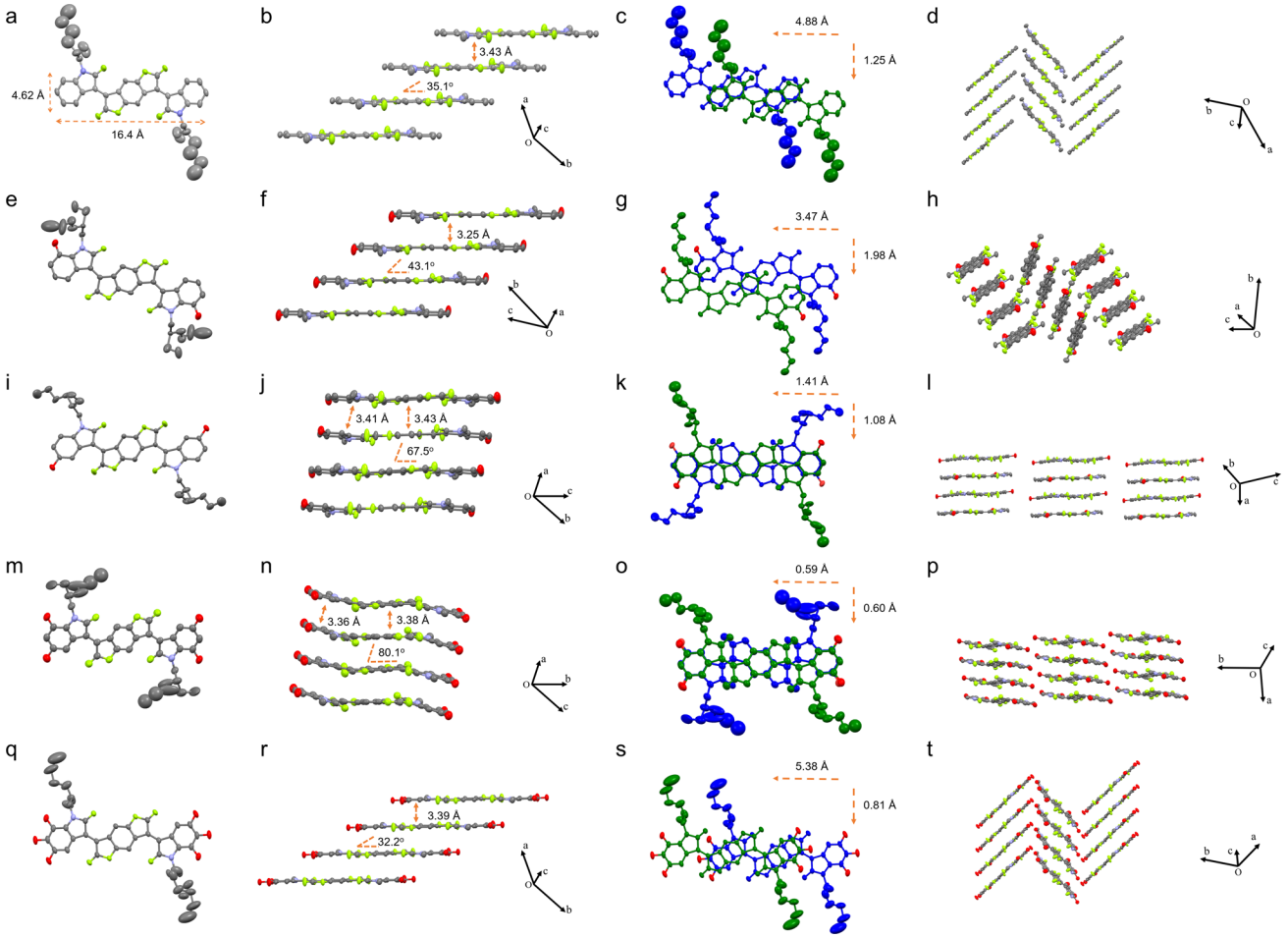

Figure 3. Crystal structures of the five BDOPV derivatives at 180 K. Thermal ellipsoids are set at 50% probability. The red-, yellow-, purple-, and gray-colored atoms represent F, O, N, and C, respectively. All of the hydrogen atoms have been omitted for clarity. (a, e, i, m, q) ORTEP structures of the five BDOPV derivatives: (a) BDOPV; (e) *o*-F_2-BDOPV; (i) *p*-F_2-BDOPV; (m) F_4-BDOPV; (q) F_6-BDOPV. (b, f, j, n, r) Molecular packing in single crystals of the five BDOPV derivatives: (b) BDOPV ($R\bar{3}$ space group, $\pi-\pi$ distance of 3.43 Å, slipping angle of 35.1°); (f) *o*-F_2-BDOPV ($P\bar{1}$ space group, $\pi-\pi$ distance of 3.25 Å, slipping angle of 43.1°); (j) *p*-F_2-BDOPV ($P\bar{1}$ space group, $\pi-\pi$ distances of 3.41 and 3.43 Å, slipping angle of 67.5°); (n) F_4-BDOPV ($P\bar{1}$ space group, $\pi-\pi$ distances of 3.36 and 3.38 Å, slipping angle of 80.1°); (r) F_6-BDOPV ($R\bar{3}$ space group, $\pi-\pi$ distance of 3.39 Å, slipping angle of 32.2°). For clarity, alkyl chains have been omitted. (c, g, k, o, s) Packing modes of two adjacent molecules along the $\pi-\pi$-stacking direction placed in the stacking geometry and their corresponding longitudinal and transverse shifts. (d, h, l, p, t) Molecular packing arrangements of the five BDOPV derivatives: (d) BDOPV (slipped 1D stacking); (h) *o*-F_2-BDOPV (herringbone arrangement); (l) *p*-F_2-BDOPV (antiparallel cofacial stacking); (p) F_4-BDOPV (antiparallel cofacial stacking); (t) F_6-BDOPV (slipped 1D stacking).

electron microscopy (SEM) and optical microscopy (OM) images (Figure S7), BDOPV and F_6-BDOPV crystals exhibited a regular, elongated hexagonal shape with lengths of over 500 μm. However, *o*-F_2-BDOPV, *p*-F_2-BDOPV, and F_4-BDOPV crystals were more inclined to show compressed hexagonal prisms (Figure S7b–d). These crystals appeared as thin slices with dark black color of millimeter-size dimension. By measuring the $\pi-\pi$ distance (d), the pitch angle (P), and the roll angle (R) (see Figure S11), the longitudinal (long molecular axis) and transverse (short molecular axis) shifts of five BDOPV single crystals were calculated according to the

DOI: 10.1021/jacs.5b11114
J. Am. Chem. Soc. 2015, 137, 15947–15956

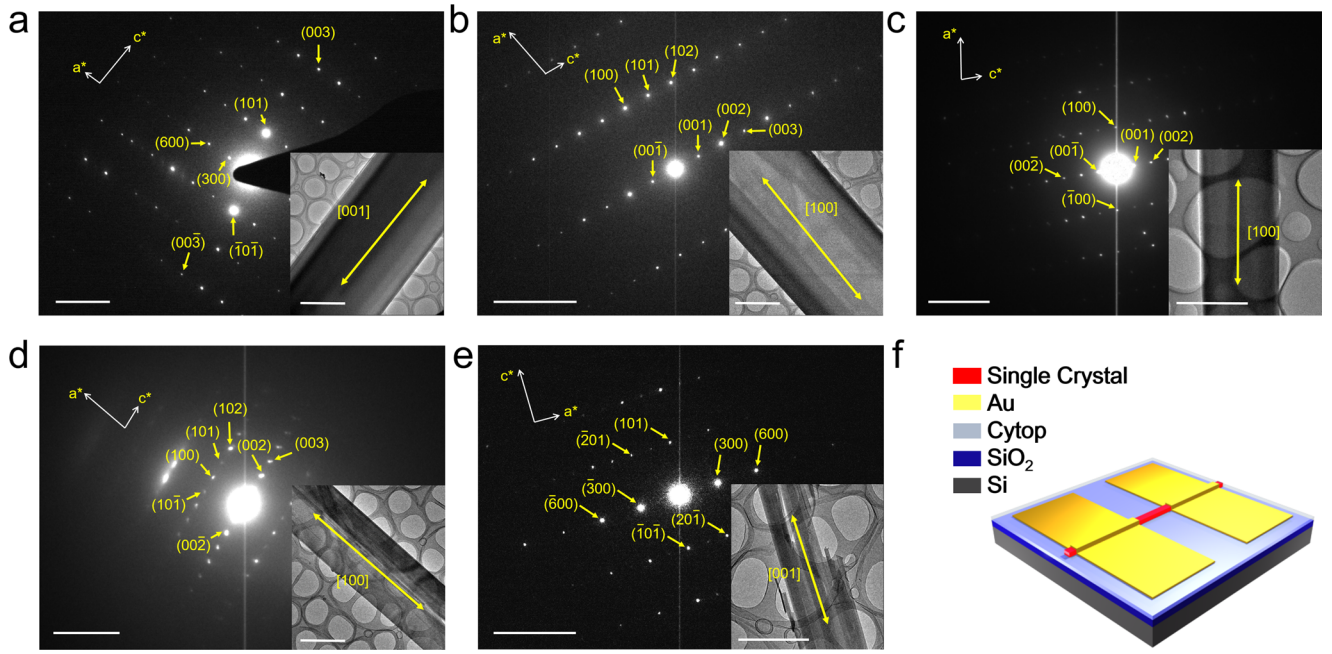

Figure 4. SAED patterns of (a) BDOPV, (b) *o*-F_2-BDOPV, (c) *p*-F_2-BDOPV, (d) F_4-BDOPV, and (e) F_6-BDOPV single crystals (scale bars: 2 nm^{-1}) and (insets) the corresponding transmission electron microscopy images (scale bars: 2 μm). The energetically preferred growth direction of the (a) BDOPV and (e) F_6-BDOPV crystals is the [001] direction (*c* axis), and that of the (b) *o*-F_2-BDOPV, (c) *p*-F_2-BDOPV, and (d) F_4-BDOPV crystals is the [100] direction (*a* axis). (f) Diagram of a BG/TC SC-OFET device with a 230 nm Cytop layer as the dielectric layer.

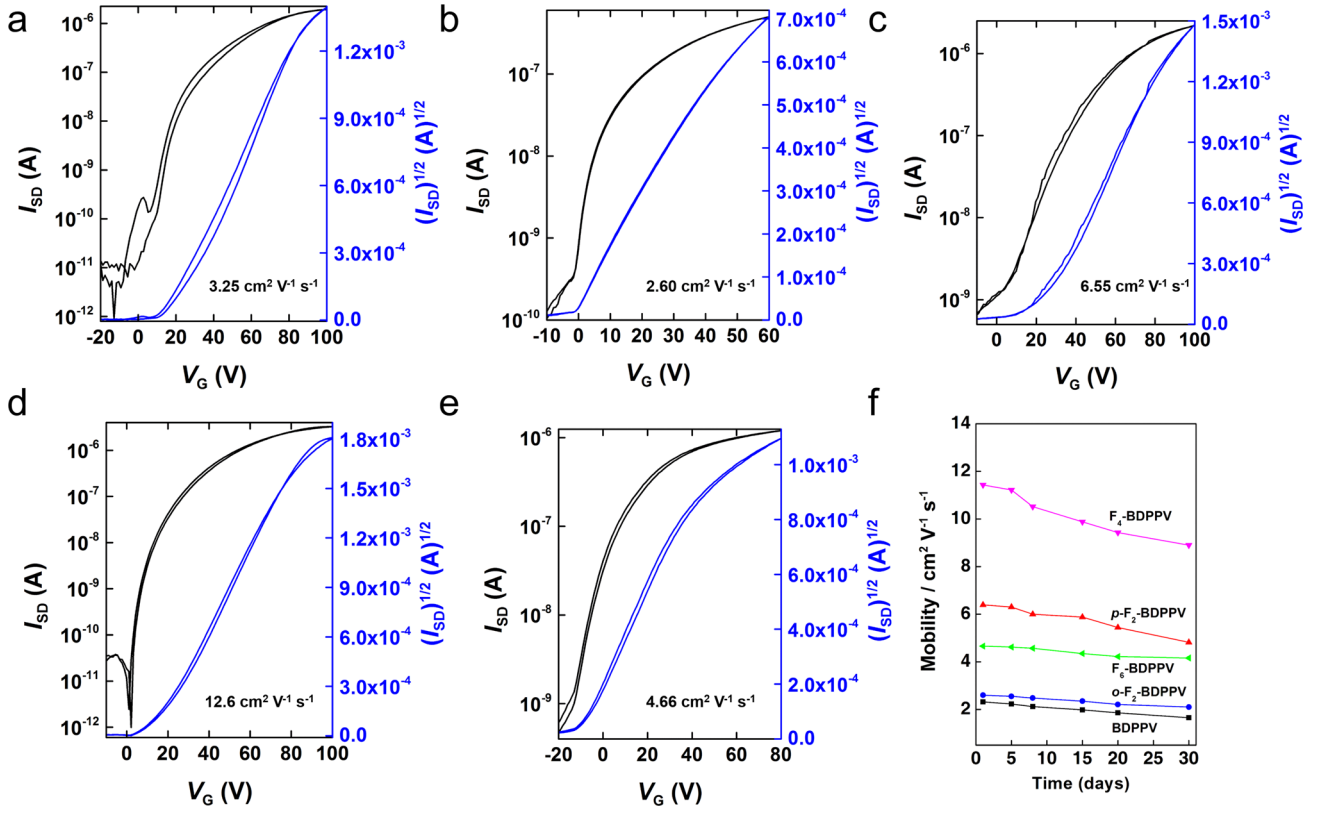

Figure 5. Transfer curves for the (a) BDOPV, (b) *o*-F_2-BDOPV, (c) *p*-F_2-BDOPV, (d) F_4-BDOPV, and (e) F_6-BDOPV devices. (f) Stabilities of the devices in air at room temperature (RH = 50−60%).

method reported by Curtius and co-workers.[48,49] The detailed crystallographic data are summarized in Tables 1 and S2.

All five molecules showed column packing with small $\pi-\pi$ distances ranging from 3.25 to 3.43 Å due to the large π planes (Figure 3). Thanks to the intramolecular hydrogen bonds, relatively planar π planes were realized in these BDOPV derivatives (Figures S8 and S9). In the single crystal of BDOPV, the molecules are arranged in a slipped 1D stacking

DOI: 10.1021/jacs.5b11114
J. Am. Chem. Soc. 2015, 137, 15947−15956

structure with a high longitudinal shift of 4.88 Å and a transverse shift of 1.25 Å between adjacent molecules (Figure 3c). Only half of each BDOPV molecular skeleton overlaps with the adjacent molecules with a slipping angle of 35.1° along the *c* axis (Figure 3b and Table 1). This is also the case for F_6-BDOPV, in which all of the hydrogen atoms on the periphery of the BDOPV backbones are substituted with fluorine atoms. The transverse shift of F_6-BDOPV is decreased to 0.81 Å, but the long-axis displacement becomes larger (5.38 Å), thus generating a small slipping angle of 32.2° (Figure 3r,s).

After the introduction of two fluorine atoms at the ortho positions of BDOPV, the longitudinal shift of *o*-F_2-BDOPV is 3.47 Å. This slightly smaller than that of BDOPV, indicating increased intermolecular overlaps along the long axis, which is consistent with the relatively larger slipping angle of 43.1° (Figure 3f,g). On the other hand, the transverse shift is increased to 1.98 Å compared with BDOPV (Figure 3g). In addition, C−H···O and C···O interactions are also found between columns, indicating the formation of an edge-to-face herringbone packing structure (Figure S10f).

p-F_2-BDOPV with two fluorine atoms introduced at the para positions and F_4-BDOPV with four fluorine atoms at both the para and ortho positions show a drastic change in the solid-state packing from slipped stacking in BDOPV single crystals to an unusual antiparallel cofacial stacking structure (Figure 3k,o).[11,50] In contrast to the severe slipping distances in the BDOPV and F_6-BDOPV single crystals, *p*-F_2-BDOPV exhibits a moderate longitudinal shift of 1.41 Å and transverse shift of 1.08 Å (Figure 3k) and thus a relatively large slipping angle of 67.5° (Figure 3j). For F_4-BDOPV, an even smaller longitudinal shift of only 0.587 Å and transverse shift of 0.601 Å (Figure 3o) and a larger slipping angle of 80.1° (Figure 3n) are realized, resulting in antiparallel cofacial packing (Figure 3o).

Single-Crystal Device Fabrication. The selected-area electron diffraction (SAED) patterns for the five crystals were indexed with the lattice constants obtained from the above single-crystal X-ray structure analysis (Figure 4a−e). The results showed that the preferential growth direction is along the [001] direction for the BDOPV and F_6-BDOPV crystals but along the [100] direction for the *o*-F_2-BDOPV, *p*-F_2-BDOPV, and F_4-BDOPV crystals; they are thus all along the π-stacking direction, which is in accordance with the Wulff plots calculated using the Bravais−Fredel−Donnay−Harker (BFDH) approach (Figure S12a−e). To test the carrier mobilities of the five molecules, bottom gate/top contact (BG/TC) single-crystal devices (Figure 4f) were fabricated according to the "plastic wire shadow mask" method (Figure S13).[51] Microwires of the five molecules were deposited on Cytop-modified SiO_2/Si substrates via a spin-coating process, and Au source and drain electrodes were deposited via thermal evaporation (Figure S14). All five single crystals exhibited typical n-type transfer and output characteristics under ambient conditions (Figures 5a−e and S15). The nonlinear behavior in the low-V_{DS} regime of the output curves indicates some contact issues in the BDOPV-derivative-based single-crystal OFET (SC-OFET) devices (Figure S16). The electron mobilities of F_4-BDOPV and *p*-F_2-BDOPV reached impressive values of 12.6 $cm^2\ V^{-1}\ s^{-1}$ (average = 7.58 $cm^2\ V^{-1}\ s^{-1}$) and 6.55 $cm^2\ V^{-1}\ s^{-1}$ (average = 3.86 $cm^2\ V^{-1}\ s^{-1}$), respectively, under ambient conditions, which are among the highest electron mobilities ever reported for air-stable SC-OFETs.[52−55] In contrast, BDOPV, *o*-F_2-BDOPV, and F_6-BDOPV showed relatively lower mobilities of 3.25 $cm^2\ V^{-1}\ s^{-1}$ (average = 1.90 $cm^2\ V^{-1}\ s^{-1}$), 2.60 $cm^2\ V^{-1}\ s^{-1}$ (average = 1.63 $cm^2\ V^{-1}\ s^{-1}$), and 4.66 $cm^2\ V^{-1}\ s^{-1}$ (average = 3.25 $cm^2\ V^{-1}\ s^{-1}$), respectively. The histograms of the electron mobilities for 22 devices for each molecule measured under ambient conditions are displayed in Figure S17. The channel width (W) and length (L) for the best device for each of the five single crystals were determined from the SEM images (Figure S14), and all of the device data are summarized in Table 2. Moreover, all of the single-crystal devices exhibited good stability in air. A typical evolution of performance versus storage time is shown in Figure 5f. Less than 25% degradation was observed when the device was kept in air (relative humidity (RH) = 50−60%) for 30 days.

Table 2. Summary of BDOPV Single-Crystal Device Performance

molecule	μ ($cm^2\ V^{-1}\ s^{-1}$)[a]	V_T (V)[b]	I_{on}/I_{off}
BDOPV	3.25 (1.90)	7.91 (5.41)	$>10^6$
o-F_2-BDOPV	2.60 (1.63)	0.52 (2.89)	$>10^3$
p-F_2-BDOPV	6.55 (3.86)	11.54 (−0.22)	$>10^3$
F_4-BDOPV	12.6 (7.58)	8.71 (3.14)	$>10^6$
F_6-BDOPV	4.66 (3.25)	−8.38 (6.49)	$>10^3$

[a]Electron mobilities measured under ambient conditions (RH = 50−60%). Shown are the maximum electron mobility values with the average values (for 22 devices) given in parentheses. [b]Threshold voltages. The average values are given in parentheses.

To obtain an in-depth understanding of the relationship between the charge transport properties of the SC-OFET devices and the packing modes of the single crystals, we carried out density functional theory (DFT) calculations on the five systems (Figure 6 and Table S3). Whether charge transport occurs through a bandlike or hopping mechanism, the reorganization energy (λ) and transfer integral (t) play vital roles in determining the carrier mobility.[9] Theoretically, a high transfer integral and small reorganization energy are favorable for high carrier mobility.[56] The electron reorganization energies of the five molecules are similar at around 0.34 eV (Figure 6b). The transfer integrals for electron transfer were calculated for the nearest-neighbor pairs along the π direction (the *c* axis for BDOPV and F_6-BDOPV and the *a* axis for *o*-F_2-BDOPV, *p*-F_2-BDOPV, and F_4-BDOPV) (Figure 6a). Higher transfer integrals are obtained in the molecular systems with smaller displacements and shorter $\pi-\pi$ stacking distances (Figure 6a). In particular, F_4-BDOPV single crystals with antiparallel cofacial stacking of the shortest displacements along the molecular axes shows the highest transfer integral, as large as 201.3 meV, which is among the highest values reported for organic semiconductors.[57] Because of the small transverse shift, a relatively high transfer integral is achieved for F_6-BDOPV with slipped 1D stacking. While BDOPV and *p*-F_2-BDOPV have the same interplanar distance, *p*-F_2-BDOPV presents a much higher transfer integral than BDOPV because of its smaller displacements as a result of the antiparallel cofacial stacking. Our calculations showed that the single crystals of the five molecules also have a great difference in the interactions between adjacent column stacks. Except for *o*-F_2-BDOPV with herringbone stacking, which shows a transfer integral of 15 meV between columns, the interstack transfer integrals for the other four molecules are extremely small. It has been found that the interstack interactions can diminish the charge transport performance along the stacking direction.[58] The electronic interference between columns might account for the lowest

DOI: 10.1021/jacs.5b11114
J. Am. Chem. Soc. 2015, 137, 15947−15956

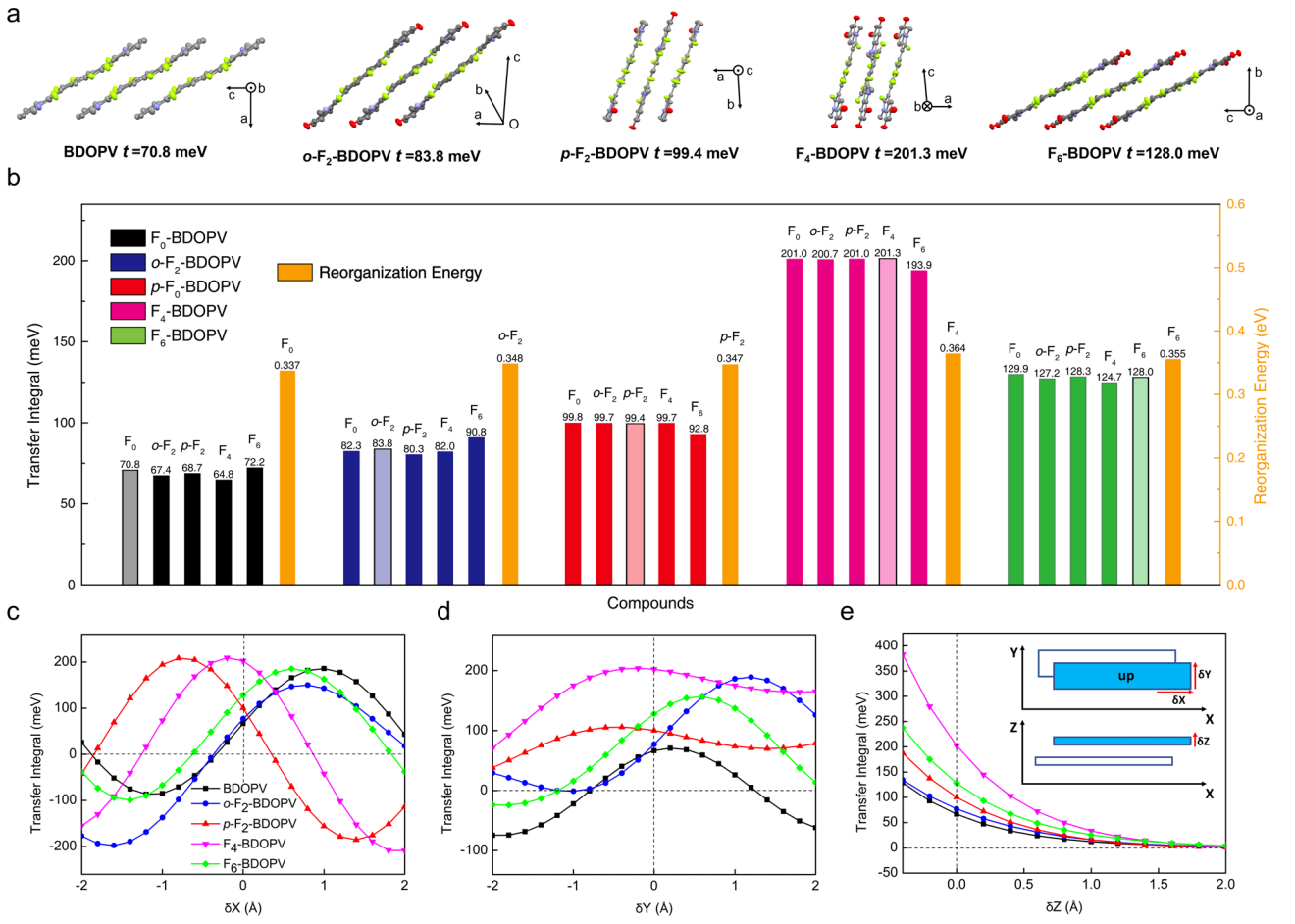

Figure 6. (a) Calculated transfer integrals for electrons of the five single crystals along the π-stacking direction. (b) Calculated transfer integrals for the five molecules adopting the same packing geometry. For example, the transfer integral of the F_0-BDOPV single crystal along the π-stacking direction was calculated to be 70.8 meV. We directly added two fluorine atoms on the BDOPV single-crystal geometry (o-F_2 or p-F_2), and the transfer integrals of these molecules under the packing mode of the BDOPV single crystal were found to be 67.4 and 68.7 meV, respectively. Including four fluorine atoms on BDOPV (F_4) gives a transfer integral of 64.8 meV, and including six fluorine atoms on BDOPV (F_6) gives a transfer integral of 72.2 meV. (c–e) Evolution of the calculated transfer integrals for electron transfer in their corresponding single-crystal packing geometries as functions of the degree of translation of one molecule along its (c) long axis, (d) short axis, and (e) intermolecular distance. The inset in (e) shows a diagram of the long axis, short axis, and intermolecular distance.

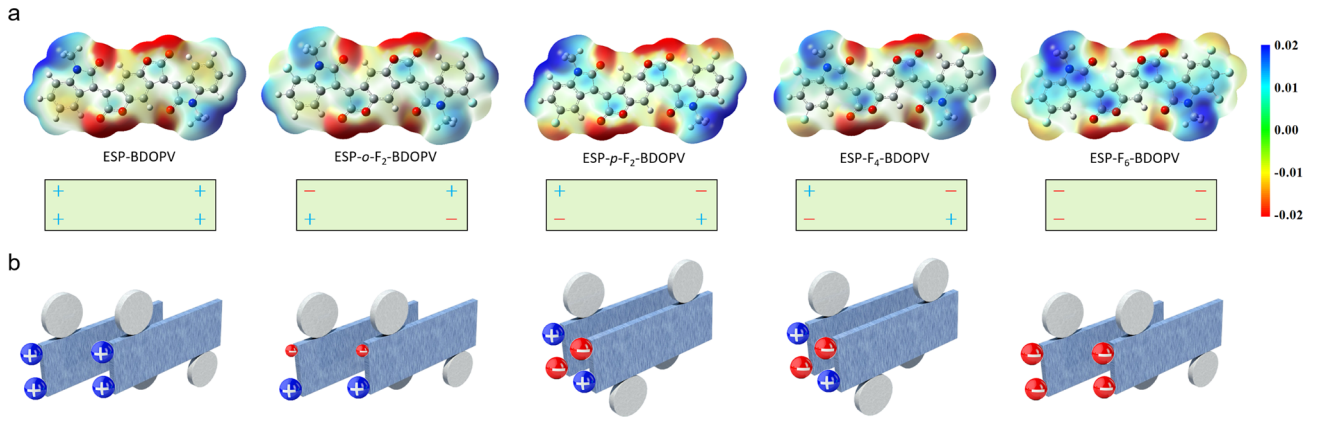

Figure 7. (a) ESP maps of the five BDOPV derivatives (all of the alkyl chains were substituted with methyl groups) and the corresponding representative charge distribution diagrams. (b) Diagrams of the molecular packing of the five BDOPV molecules (positive signs indicate positive potential, and negative signs indicate negative potential).

electron mobility in the single crystal of o-F_2-BDOPV even though it has larger transfer integrals with respect to the BDOPV crystal. It is important to note that small changes in displacements can lead to significant changes in the magnitude of transfer integrals,[59,60] as revealed by the transfer integral evolutions along the long and short axes (Figure 6c–e). Among

DOI: 10.1021/jacs.5b11114
J. Am. Chem. Soc. 2015, 137, 15947–15956

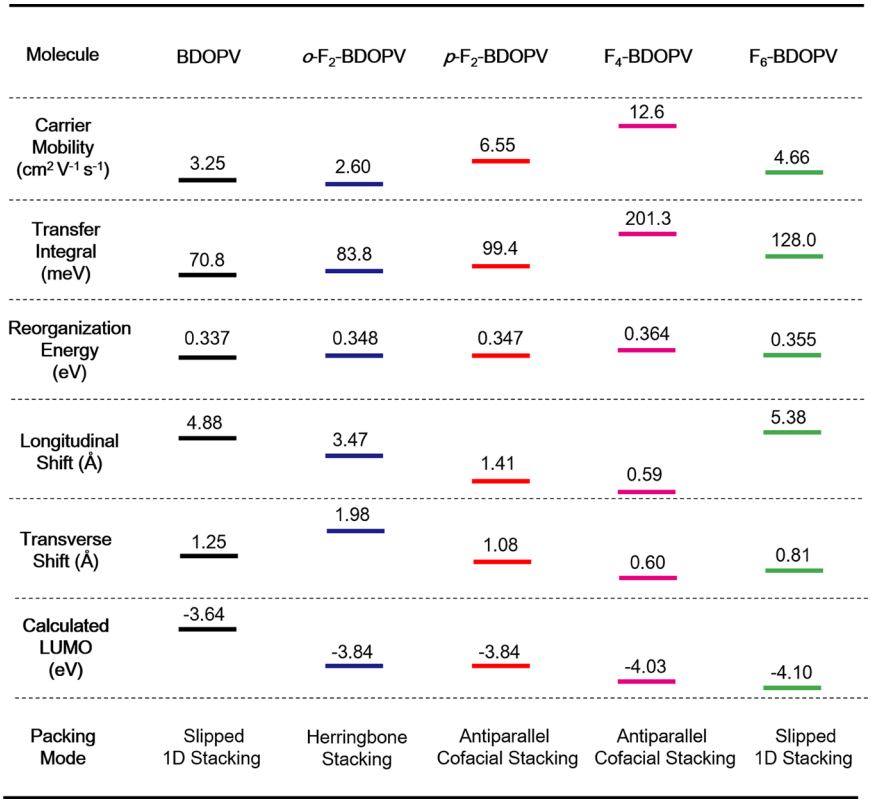

Figure 8. Summary of physical properties, crystal packing modes, and SC-OFET performance of the five BDOPV derivatives.

all of the studied single crystals, the transfer integral of F_4-BDOPV in the experimental stacking geometry is close to the best estimated value, indicating the ideal of the antiparallel cofacial stacking for F_4-BDOPV. On the other hand, the other single crystals show intermediate transfer integrals in their original crystal packing modes with relatively large displacements. Furthermore, as can be seen from Figure 6b, replacing the hydrogen atoms with fluorine or vice versa has hardly any influence on the transfer integrals for compounds that adopt the same packing mode, indicating that the sharp contrast of electronic couplings in the five single crystals arises mainly from the distinct packing modes. The larger packing density, short $\pi-\pi$ distances, and the smallest longitudinal and transverse shifts contribute cooperatively to the realization of the largest transfer integral in the single crystal of F_4-BDOPV. On the other hand, the LUMO levels of the five molecules are all very low and do not influence the electron mobilities. By and large, the electron mobilities among the five molecules are consistent with the electronic couplings in their crystal structures.

Fluorine-Induced Charge Distribution and Impact on Crystal Packing. The electrostatic potential (ESP) is widely used to visualize and understand the non-covalent interactions of organic molecules.[37,61−63] In order to find out the reason for the change in crystal packing of the five BDOPV derivatives, we calculated the ESP maps of the five molecules (Figure 7a). For BDOPV, the negative potential is mainly exhibited on oxygen atoms because of the electron-withdrawing property of carbonyl groups, concentrating on the middle of the longitudinal sides of the molecule, while the two lateral sides of the molecule show positive potentials because of the lower electronegativity of hydrogen than carbon (Figure 7a). Upon substitution of all six peripheral hydrogen atoms with fluorine, the ESPs around the periphery are changed to negative thanks to the largest Pauling atomic electronegativity of fluorine atoms (Figure 7a). In order to maximize electrostatic attraction/minimize electrostatic repulsion and avoid steric hindrance between alkyl chains, BDOPV and F_6-BDOPV molecules tend to adopt parallel stacking with severe slippages (Figures 3c,s, 7b, and S18). After the selective introduction of fluorine atoms, the ESPs on the four terminals of p-F_2-BDOPV and F_4-BDOPV are changed with the same sign of potentials on the same longitudinal or lateral sides (Figure 7a). Benefiting from the attractive Coulomb interactions between the terminal charges, the adjacent molecules tend to associate with each other in an antiparallel cofacial packing mode (Figures 3k,o and 7b).[61,62] Such an antiparallel packing mode can significantly decrease the dislocation along the long and short axes. Moreover, electron-withdrawing substituents can diminish the electron density, leading to weaker intermolecular electrostatic repulsion and thus smaller $\pi-\pi$ stacking distances in the single crystals of F_4-BDOPV (Figure 3n).[64] On the other hand, since the alkyl chains are substituted on the BDOPV backbone in a staggered way, such antiparallel cofacial stacking can avoid suffering from the steric hindrance effects that often appear for the molecular systems showing substituted alkyl chains without dislocation, such as TIPS-pentacene[23] and β-phase Cl_2-NDI[26] (Figures 1a and S1). It is interesting to make comparison between p-F_2-BDOPV and o-F_2-BDOPV. For o-F_2-BDOPV, the fluorine atoms are introduced adjacent to the alkyl chains, and therefore, the positive potentials of the alkyl chains compensate for the negative potentials induced by fluorine. However, in the case of p-F_2-BDOPV, the fluorine atoms are introduced far away from the alkyl chains and hence can induce much stronger negative potentials (Figure 7a). Therefore, although the charge distribution in o-F_2-BDOPV seems to be the same type as that in F_4-BDOPV (Figure 7a), the single-crystal stacking mode

DOI: 10.1021/jacs.5b11114
J. Am. Chem. Soc. 2015, 137, 15947−15956

is very different from that of *p*-F_2-BDOPV and F_4-BDOPV; instead, it shows a herringbone motif composed of slipped parallel stacks (Figure 3h). This is mainly due to the relatively weak negative and positive potentials on the periphery of the conjugated backbone, which are unable to provide enough attractive electrostatic interaction (Figure 7b).[65,66] To conclude, our results demonstrate that the non-covalent interactions and thus the intermolecular packing modes can be fine-tuned by the introduction of fluorine atoms.

CONCLUSION

We have successfully realized a high degree of control over molecular packing through the strategy of tuning the charge distribution and obtained a series of new n-type organic molecules based on BDOPV. By the incorporation of different numbers of fluorine atoms at various positions on the BDOPV backbone, five n-type molecules, BDOPV, *o*-F_2-BDOPV, *p*-F_2-BDOPV, F_4-BDOPV, and F_6-BDOPV, present distinct displacements and interplanar distances with similar column packing motifs in single crystals (Figure 8). BDOPV and F_6-BDOPV with similar charge distributions tend to stack between each other with large displacements to avoid electrostatic repulsion, thus forming slipped 1D packing. Upon the incorporation of fluorine atoms at proper positions, the charge distributions of *p*-F_2-BDOPV and F_4-BDOPV are changed. To maximize the electrostatic interactions, they adopt an unusual antiparallel cofacial stacking motif with small displacements along both the long and short axises and short $\pi-\pi$ stacking distances. The staggered substituted alkyl chains do not cause any extra steric effect in cofacial stacking. The small displacement and close $\pi-\pi$ stacking distance in antiparallel stacking result in larger transfer integrals and thus higher electron mobilities than those of molecules adopting slipped stacking (Figure 8). The column stacking with face-to-face interactions and low enough LUMO levels cause all five BDOPV derivatives to show air-stable electron mobilities of over 2 $cm^2\ V^{-1}\ s^{-1}$. These systematically high electron mobilities appearing in a single molecular system have never been observed before, suggesting the broad application of BDOPV derivatives in n-type materials. More importantly, our work demonstrates that tuning of the charge distribution of the molecular backbone is a versatile and effective method to fine-tune the molecular packing in organic single crystals.

ASSOCIATED CONTENT

Supporting Information

The Supporting Information is available free of charge on the ACS Publications website at DOI: 10.1021/jacs.5b11114.

Experimental details, characterization data, NMR spectra, Figures S1−S18, and Tables S1−S3 (PDF)
Crystallographic data in CIF format (ZIP)

AUTHOR INFORMATION

Corresponding Authors

*ypyi@iccas.ac.cn
*jieyuwang@pku.edu.cn
*jianpei@pku.edu.cn

Author Contributions

§J.-H.D. and Y.-Q.Z. contributed equally.

Notes

The authors declare no competing financial interest.

ACKNOWLEDGMENTS

This work was supported by the Major State Basic Research Development Program (2013CB933501 and 2015CB856505) from MOST, the National Natural Science Foundation of China, the Beijing Natural Science Foundation (2144049), and the Strategic Priority Research Program of the Chinese Academy of Sciences (Grant XDB12020200). The authors thank beamline BL14B1 and BL17U1 at the Shanghai Synchrotron Radiation Facility for providing the beam time. The authors also thank Prof. Jian-Rong Li and Dr. Minjian Zhao (Beijing University of Technology) for their kind help with the single-crystal X-ray diffraction tests.

REFERENCES

(1) Mas-Torrent, M.; Rovira, C. *Chem. Rev.* **2011**, *111*, 4833−4856.
(2) Dou, L.; You, J.; Hong, Z.; Xu, Z.; Li, G.; Street, R. A.; Yang, Y. *Adv. Mater.* **2013**, *25*, 6642−6671.
(3) Facchetti, A. *Chem. Mater.* **2011**, *23*, 733−758.
(4) Zhang, L.; Liu, F.; Diao, Y.; Marsh, H. S.; Colella, N. S.; Jayaraman, A.; Russell, T. P.; Mannsfeld, S. C. B.; Briseno, A. L. *J. Am. Chem. Soc.* **2014**, *136*, 18120−18130.
(5) Zhang, L.; Colella, N. S.; Liu, F.; Trahan, S.; Baral, J. K.; Winter, H. H.; Mannsfeld, S. C. B.; Briseno, A. L. *J. Am. Chem. Soc.* **2013**, *135*, 844−854.
(6) Bendikov, M.; Wudl, F.; Perepichka, D. F. *Chem. Rev.* **2004**, *104*, 4891−4945.
(7) Hartnett, P. E.; Timalsina, A.; Matte, H. S. S. R.; Zhou, N.; Guo, X.; Zhao, W.; Facchetti, A.; Chang, R. P. H.; Hersam, M. C.; Wasielewski, M. R.; Marks, T. J. *J. Am. Chem. Soc.* **2014**, *136*, 16345−16356.
(8) Sirringhaus, H. *Adv. Mater.* **2014**, *26*, 1319−1335.
(9) Coropceanu, V.; Cornil, J.; da Silva Filho, D. A.; Olivier, Y.; Silbey, R.; Brédas, J.-L. *Chem. Rev.* **2007**, *107*, 926−952.
(10) Feng, X.; Marcon, V.; Pisula, W.; Hansen, M. R.; Kirkpatrick, J.; Grozema, F.; Andrienko, D.; Kremer, K.; Müllen, K. *Nat. Mater.* **2009**, *8*, 421−426.
(11) Dong, H.; Fu, X.; Liu, J.; Wang, Z.; Hu, W. *Adv. Mater.* **2013**, *25*, 6158−6183.
(12) Anthony, J. E. *Angew. Chem., Int. Ed.* **2008**, *47*, 452−483.
(13) Takimiya, K.; Osaka, I.; Mori, T.; Nakano, M. *Acc. Chem. Res.* **2014**, *47*, 1493−1502.
(14) Zhang, L.; Fonari, A.; Liu, Y.; Hoyt, A.-L. M.; Lee, H.; Granger, D.; Parkin, S.; Russell, T. P.; Anthony, J. E.; Brédas, J.-L.; Coropceanu, V.; Briseno, A. L. *J. Am. Chem. Soc.* **2014**, *136*, 9248−9251.
(15) Briseno, A. L.; Miao, Q.; Ling, M.-M.; Reese, C.; Meng, H.; Bao, Z.; Wudl, F. *J. Am. Chem. Soc.* **2006**, *128*, 15576−15577.
(16) Jiang, H.; Zhao, H.; Zhang, K. K.; Chen, X.; Kloc, C.; Hu, W. *Adv. Mater.* **2011**, *23*, 5074−5080.
(17) Zheng, Y.; Miao, M.-S.; Zhang, Y.; Nguyen, T.-Q.; Wudl, F. *J. Am. Chem. Soc.* **2014**, *136*, 11614−11617.
(18) Park, J.-I.; Chung, J. W.; Kim, J.-Y.; Lee, J.; Jung, J. Y.; Koo, B.; Lee, B.-L.; Lee, S. W.; Jin, Y. W.; Lee, S. Y. *J. Am. Chem. Soc.* **2015**, *137*, 12175−12178.
(19) Gsänger, M.; Oh, J. H.; Könemann, M.; Höffken, H. W.; Krause, A.-M.; Bao, Z.; Würthner, F. *Angew. Chem., Int. Ed.* **2010**, *49*, 740−743.
(20) Schmidt, R.; Ling, M. M.; Oh, J. H.; Winkler, M.; Könemann, M.; Bao, Z.; Würthner, F. *Adv. Mater.* **2007**, *19*, 3692−3695.
(21) Zhang, F.; Hu, Y.; Schuettfort, T.; Di, C.-A.; Gao, X.; McNeill, C. R.; Thomsen, L.; Mannsfeld, S. C. B.; Yuan, W.; Sirringhaus, H.; Zhu, D. *J. Am. Chem. Soc.* **2013**, *135*, 2338−2349.
(22) Miao, Q.; Chi, X.; Xiao, S.; Zeis, R.; Lefenfeld, M.; Siegrist, T.; Steigerwald, M. L.; Nuckolls, C. *J. Am. Chem. Soc.* **2006**, *128*, 1340−1345.
(23) Anthony, J. E.; Brooks, J. S.; Eaton, D. L.; Parkin, S. R. *J. Am. Chem. Soc.* **2001**, *123*, 9482−9483.

DOI: 10.1021/jacs.5b11114
J. Am. Chem. Soc. 2015, 137, 15947−15956

(24) Ryno, S. M.; Risko, C.; Brédas, J.-L. *J. Am. Chem. Soc.* **2014**, *136*, 6421−6427.
(25) Ebata, H.; Izawa, T.; Miyazaki, E.; Takimiya, K.; Ikeda, M.; Kuwabara, H.; Yui, T. *J. Am. Chem. Soc.* **2007**, *129*, 15732−15733.
(26) He, T.; Stolte, M.; Burschka, C.; Hansen, N. H.; Musiol, T.; Kälblein, D.; Pflaum, J.; Tao, X.; Brill, J.; Würthner, F. *Nat. Commun.* **2015**, *6*, 5954.
(27) Jiang, W.; Li, Y.; Wang, Z. *Chem. Soc. Rev.* **2013**, *42*, 6113−6127.
(28) Wang, C.; Dong, H.; Hu, W.; Liu, Y.; Zhu, D. *Chem. Rev.* **2012**, *112*, 2208−2267.
(29) Usta, H.; Facchetti, A.; Marks, T. J. *Acc. Chem. Res.* **2011**, *44*, 501−510.
(30) Kim, F. S.; Ren, G.; Jenekhe, S. A. *Chem. Mater.* **2011**, *23*, 682−732.
(31) Mei, J.; Diao, Y.; Appleton, A. L.; Fang, L.; Bao, Z. *J. Am. Chem. Soc.* **2013**, *135*, 6724−6746.
(32) Tang, M. L.; Bao, Z. *Chem. Mater.* **2011**, *23*, 446−455.
(33) Babudri, F.; Farinola, G. M.; Naso, F.; Ragni, R. *Chem. Commun.* **2007**, 1003−1022.
(34) Sakamoto, Y.; Suzuki, T.; Kobayashi, M.; Gao, Y.; Fukai, Y.; Inoue, Y.; Sato, F.; Tokito, S. *J. Am. Chem. Soc.* **2004**, *126*, 8138−8140.
(35) Tang, M. L.; Reichardt, A. D.; Wei, P.; Bao, Z. *J. Am. Chem. Soc.* **2009**, *131*, 5264−5273.
(36) Reichenbächer, K.; Süss, H. I.; Hulliger, J. *Chem. Soc. Rev.* **2005**, *34*, 22−30.
(37) Pace, C. J.; Gao, J. *Acc. Chem. Res.* **2013**, *46*, 907−915.
(38) Lei, T.; Xia, X.; Wang, J.-Y.; Liu, C.-J.; Pei, J. *J. Am. Chem. Soc.* **2014**, *136*, 2135−2141.
(39) Facchetti, A.; Yoon, M.-H.; Stern, C. L.; Katz, H. E.; Marks, T. J. *Angew. Chem., Int. Ed.* **2003**, *42*, 3900−3903.
(40) Swartz, C. R.; Parkin, S. R.; Bullock, J. E.; Anthony, J. E.; Mayer, A. C.; Malliaras, G. G. *Org. Lett.* **2005**, *7*, 3163−3166.
(41) Chen, Z.; Müller, P.; Swager, T. M. *Org. Lett.* **2006**, *8*, 273−276.
(42) Lei, T.; Wang, J.-Y.; Pei, J. *Acc. Chem. Res.* **2014**, *47*, 1117−1126.
(43) Lei, T.; Dou, J.-H.; Cao, X.-Y.; Wang, J.-Y.; Pei, J. *J. Am. Chem. Soc.* **2013**, *135*, 12168−12171.
(44) Dou, J.-H.; Zheng, Y.-Q.; Yao, Z.-F.; Lei, T.; Shen, X.; Luo, X.-Y.; Yu, Z.-A.; Zhang, S.-D.; Han, G.; Wang, Z.; Yi, Y.; Wang, J.-Y.; Pei, J. *Adv. Mater.* **2015**, DOI: 10.1002/adma.201503803.
(45) Yan, Z.; Sun, B.; Li, Y. *Chem. Commun.* **2013**, *49*, 3790−3792.
(46) Gui, Q.; Dai, F.; Liu, J.; Chen, P.; Yang, Z.; Chen, X.; Tan, Z. *Org. Biomol. Chem.* **2014**, *12*, 3349−3353.
(47) Zang, L.; Che, Y.; Moore, J. S. *Acc. Chem. Res.* **2008**, *41*, 1596−1608.
(48) Schmidt, R.; Oh, J. H.; Sun, Y.-S.; Deppisch, M.; Krause, A.-M.; Radacki, K.; Braunschweig, H.; Könemann, M.; Erk, P.; Bao, Z.; Würthner, F. *J. Am. Chem. Soc.* **2009**, *131*, 6215−6228.
(49) Curtis, M. D.; Cao, J.; Kampf, J. W. *J. Am. Chem. Soc.* **2004**, *126*, 4318−4328.
(50) Arjona-Esteban, A.; Krumrain, K.; Liess, A.; Stolte, M.; Huang, L.; Schmidt, D.; Stepanenko, V.; Gsänger, M.; Hertel, D.; Meerholz, K.; Würthner, F. *J. Am. Chem. Soc.* **2015**, *137*, 13524−13534.
(51) Zhou, Y.; Lei, T.; Wang, L.; Pei, J.; Cao, Y.; Wang, J. *Adv. Mater.* **2010**, *22*, 1484−1487.
(52) Li, H.; Tee, B. C.-K.; Cha, J. J.; Cui, Y.; Chung, J. W.; Lee, S. Y.; Bao, Z. *J. Am. Chem. Soc.* **2012**, *134*, 2760−2765.
(53) Lv, A.; Puniredd, S. R.; Zhang, J.; Li, Z.; Zhu, H.; Jiang, W.; Dong, H.; He, Y.; Jiang, L.; Li, Y.; Pisula, W.; Meng, Q.; Hu, W.; Wang, Z. *Adv. Mater.* **2012**, *24*, 2626−2630.
(54) He, T.; Stolte, M.; Würthner, F. *Adv. Mater.* **2013**, *25*, 6951−6955.
(55) Krupskaya, Y.; Gibertini, M.; Marzari, N.; Morpurgo, A. F. *Adv. Mater.* **2015**, *27*, 2453−2458.
(56) Sokolov, A. N.; Atahan-Evrenk, S.; Mondal, R.; Akkerman, H. B.; Sánchez-Carrera, R. S.; Granados-Focil, S.; Schrier, J.; Mannsfeld, S. C. B.; Zoombelt, A. P.; Bao, Z.; Aspuru-Guzik, A. *Nat. Commun.* **2011**, *2*, 437.
(57) Yavuz, I.; Martin, B. N.; Park, J.; Houk, K. N. *J. Am. Chem. Soc.* **2015**, *137*, 2856−2866.
(58) Zhu, L.; Coropceanu, V.; Yi, Y.; Chilukuri, B.; Cundari, T. R.; Brédas, J.-L. *J. Phys. Chem. Lett.* **2013**, *4*, 2186−2189.
(59) Diao, Y.; Lenn, K. M.; Lee, W.-Y.; Blood-Forsythe, M. A.; Xu, J.; Mao, Y.; Kim, Y.; Reinspach, J. A.; Park, S.; Aspuru-Guzik, A.; Xue, G.; Clancy, P.; Bao, Z.; Mannsfeld, S. C. B. *J. Am. Chem. Soc.* **2014**, *136*, 17046−17057.
(60) Tsao, H. N.; Cho, D. M.; Park, I.; Hansen, M. R.; Mavrinskiy, A.; Yoon, D. Y.; Graf, R.; Pisula, W.; Spiess, H. W.; Müllen, K. *J. Am. Chem. Soc.* **2011**, *133*, 2605−2612.
(61) Wheeler, S. E. *J. Am. Chem. Soc.* **2011**, *133*, 10262−10274.
(62) Meyer, E. A.; Castellano, R. K.; Diederich, F. *Angew. Chem., Int. Ed.* **2003**, *42*, 1210−1250.
(63) Salonen, L. M.; Ellermann, M.; Diederich, F. *Angew. Chem., Int. Ed.* **2011**, *50*, 4808−4842.
(64) Delgado, M. C. R.; Pigg, K. R.; da Silva Filho, D. A.; Gruhn, N. E.; Sakamoto, Y.; Suzuki, T.; Osuna, R. M.; Casado, J.; Hernández, V.; Navarrete, J. T. L.; Martinelli, N. G.; Cornil, J.; Sánchez-Carrera, R. S.; Coropceanu, V.; Brédas, J.-L. *J. Am. Chem. Soc.* **2009**, *131*, 1502−1512.
(65) Dou, J.-H.; Zheng, Y.-Q.; Lei, T.; Zhang, S.-D.; Wang, Z.; Zhang, W.-B.; Wang, J.-Y.; Pei, J. *Adv. Funct. Mater.* **2014**, *24*, 6270−6278.
(66) Lei, T.; Dou, J.-H.; Pei, J. *Adv. Mater.* **2012**, *24*, 6457−6461.

DOI: 10.1021/jacs.5b11114
J. Am. Chem. Soc. 2015, 137, 15947−15956